Cell Reports
Physical Science

CellPress
OPEN ACCESS

Article

Synthesis of stable single-crystalline carbon dioxide clathrate powder by pressure swing crystallization

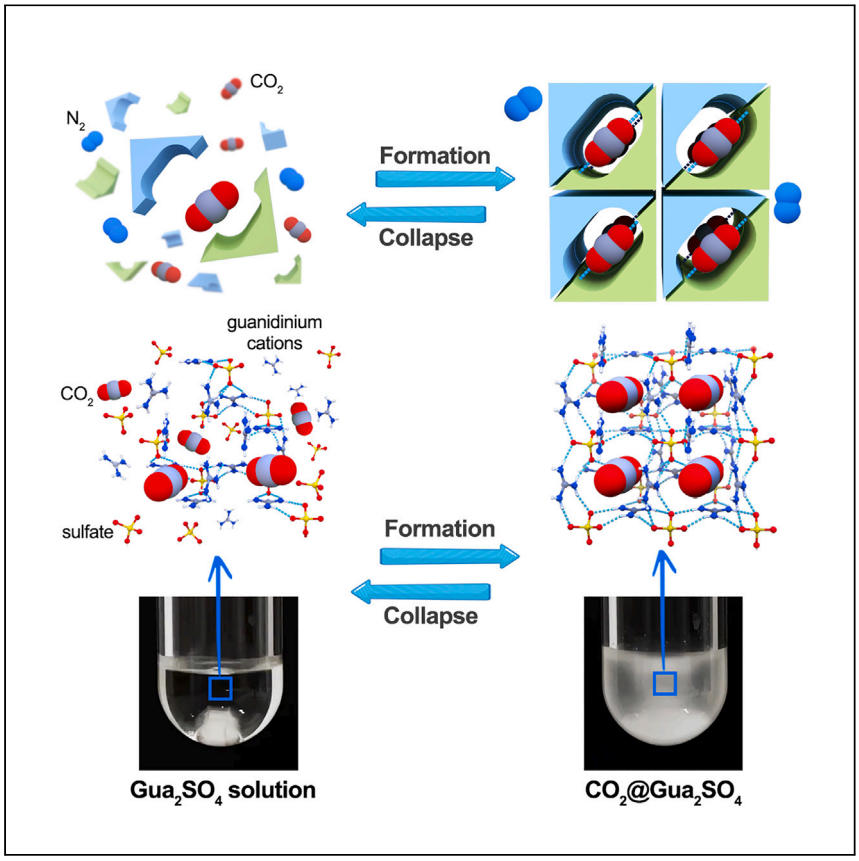

Carbon capture and storage (CCS) requires adsorbents that can efficiently capture and store CO_2 in inexpensive solid forms in order to effectively control greenhouse gas emissions. Xiang et al. synthesize a stable CO_2 inclusion salt powder from an aqueous solution of guanidinium sulfate, which can reversibly store up to 17 w/w CO_2. This enables solid CO_2 storage or transport under ambient conditions.

Zhiling Xiang, Congyan Liu, Chunhui Chen, ..., Cafer T. Yavuz, Qiang Xu, Bo Liu

cafer.yavuz@kaust.edu.sa (C.T.Y.)
xuq@sustech.edu.cn (Q.X.)
liuchem@ustc.edu.cn (B.L.)

Highlights

CO_2-selective clathrate synthesized from Gua_2SO_4 solution under ambient conditions

Single-crystalline clathrate shows high CO_2 capacity up to 17% w/w

Clathrate exhibits selectivity toward CO_2 even in presence of N_2 and water

Fast and consistent formation makes clathrate promising for gas capture and storage

Xiang et al., Cell Reports Physical Science 4, 101383
May 17, 2023
https://doi.org/10.1016/j.xcrp.2023.101383

Cell Reports
Physical Science

CellPress
OPEN ACCESS

Article

Synthesis of stable single-crystalline carbon dioxide clathrate powder by pressure swing crystallization

Zhiling Xiang,[1,5] Congyan Liu,[1,5] Chunhui Chen,[1] Xin Xiao,[2] Thien S. Nguyen,[3] Cafer T. Yavuz,[3,*] Qiang Xu,[2,4,*] and Bo Liu[1,6,*]

SUMMARY

Reversible CO_2 capture and release under ambient conditions is crucial for energy-efficient carbon capture and storage. Here, we report the pressure swing crystallization of CO_2 in a single-crystalline guanidinium sulfate-based clathrate salt under practical conditions of 52 kPa and 298 K, with a high CO_2 density (0.252 g cm^{-3}) and capacity (17 wt %). The captured CO_2 is released as a pure stream through moderate means of pressure or temperature stimulation, all while the desorbed Gua_2SO_4 is ready for another cycle. The clathrate is selective exclusively to CO_2 even in the presence of common flue gas components, such as water vapor and N_2, owing to the specific electrostatic interaction between the CO_2 and guanidinium cations. The mechanism unraveled through single-crystal studies is distinctively different from physisorption or chemisorption, opening up a promising venue for future carbon capture and storage technologies through rapid CO_2 solidification using an abundant salt.

INTRODUCTION

Reversible carbon capture and release in an energy-efficient way is vital toward many industrial processes, particularly in efforts to address the current global warming crisis. In general, CO_2 capture solutions can be classified into physisorption and chemisorption processes through temperature or pressure swing operations. But each strategy possesses its own merits and shortcomings. Physisorption of CO_2 via weak interactions mainly involves porous materials with high surface areas, such as porous carbons,[1,2] zeolites,[3,4] metal-organic frameworks,[5–7] covalent-organic frameworks,[8] and hydrogen-bonded organic frameworks,[9] giving rise to low sorption heat and easy adsorbent regeneration. Parasitic molecules like water, however, compete with CO_2 and deteriorate the selectivity, capacity, and cycling performance for carbon capture and ultimately increase the energy consumption for regeneration in practical scenarios.[10–13] Chemisorption of CO_2, on the other hand, usually produces high heat and therefore requires intensive energy input for absorbent regeneration.[14–16] This is because the captured CO_2 is converted into carbamates and carbonates (HCO_3^- or CO_3^{2-}) when brought into contact with aqueous amine solutions or tethered amines on porous supports. One example is guanidine, a multi-amine construct, which has been explored as a chemisorptive CO_2 absorbent for direct carbon capture from air.[17–20] In nature, guanidine-based CO_2 capture is a chemical conversion process taking advantage of basicity of guanidine, similar to carbon capture using alkaline solutions or monoethanolamine. This chemical product required high regeneration energy, usually at temperatures higher than 120°C.

[1]School of Chemistry and Materials Science, University of Science and Technology of China, Hefei, Anhui 230026, P.R. China

[2]Shenzhen Key Laboratory of Micro/Nano-Porous Functional Materials (SKLPM), SUSTech-Kyoto University Advanced Energy Materials Joint Innovation Laboratory (SKAEM-JIL), Department of Chemistry, Southern University of Science and Technology (SUSTech), Shenzhen 518055, P.R. China

[3]Oxide & Organic Nanomaterials for Energy & Environment (ONE) Laboratory, Chemistry Program, Advanced Membranes & Porous Materials (AMPM) Center, KAUST Catalysis Center (KCC), Physical Science & Engineering (PSE), King Abdullah University of Science and Technology (KAUST), Thuwal 23955, Saudi Arabia

[4]Institute for Integrated Cell-Material Sciences (iCeMS), Kyoto University, Kyoto 606-8501, Japan

[5]These authors contributed equally

[6]Lead contact

*Correspondence: cafer.yavuz@kaust.edu.sa (C.T.Y.), xuq@sustech.edu.cn (Q.X.), liuchem@ustc.edu.cn (B.L.)

https://doi.org/10.1016/j.xcrp.2023.101383

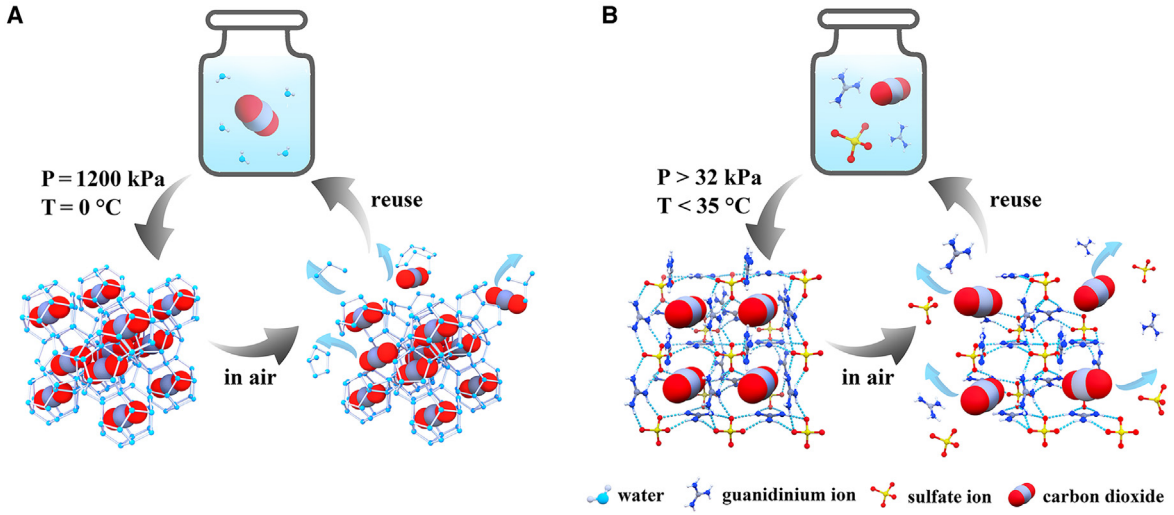

Figure 1. Schematic demonstration of reversible clathrate formations with pressure swing for CO_2 capture and release process

(A) CO_2 hydrate where CO_2 molecules are trapped in water clusters at high pressures and low temperatures.

(B) A clathrate from guanidinium sulfate and CO_2, CO_2@Gua_2SO_4, where CO_2 can be captured at pressures as low as 32 kPa and temperatures at flue gas conditions (35°C and below).

An interesting example is a 3D hydrogen-bonded framework assembled from tetrahedral tetraamidinium cations and carbonates via nonelectrostatic hydrogen bond in water,[21] but utility for a cyclic CO_2 capture through dynamic complexation is not clear.

Gas hydrates such as CO_2 hydrates are suitable for a rapid, reversible carbon capture. They are, however, often generated at low temperatures and high pressures (for example, T = 0°C and P = 1,200 kPa). In a CO_2 hydrate, CO_2 is enclosed in a water cage constructed through hydrogen bonds.[22] In other words, CO_2 forces icy water to crystallize into a hydrate framework, where it is also known to trap other guest species such as CH_4, N_2, or small organic molecules.[23] Under increasing temperature or reduced pressure, for example bringing CO_2 clathrates to ambient conditions, the water cages collapse, and trapped guest molecules escape. Laboratory syntheses of gas hydrates have been accomplished.[24] The kinetics of clathrate formation, however, remain unchanged, where the conditions of low temperature and high pressure are indispensable, making CO_2 hydrates impractical for applications of gas adsorption, separation, and storage. Recently, we reported a reversible structural transformation of $[B(OCH_3)_4]_3[C(NH_2)_3]_4Cl \cdot 4CH_3OH$ upon MeOH capture and release as an example of achieving dynamic behavior of gas hydrates at ambient conditions.[25] Carbon capture and storage as a powder based on clathrate formation using CO_2 hydrate is challenging and remains elusive, to the best of our knowledge.

Herein, we report a stable CO_2 clathrate powder formation under ambient conditions through co-crystallization of CO_2 with guanidinium sulfate (Gua_2SO_4, where Gua is guanidinium) from an aqueous Gua_2SO_4 solution (Figure 1). As revealed by our single-crystal studies, crystallization of CO_2@Gua_2SO_4 is triggered by dominant electrostatic interactions between CO_2 and guanidinium ions, which are encased among the strong hydrogen bond interactions between guanidinium cations and sulfate. CO_2@Gua_2SO_4 readily releases CO_2 through structure collapsing in ambient conditions, and the resultant Gua_2SO_4 is ready for another cycle without requiring further regeneration (Figure 1). The volume and weight densities of CO_2 in

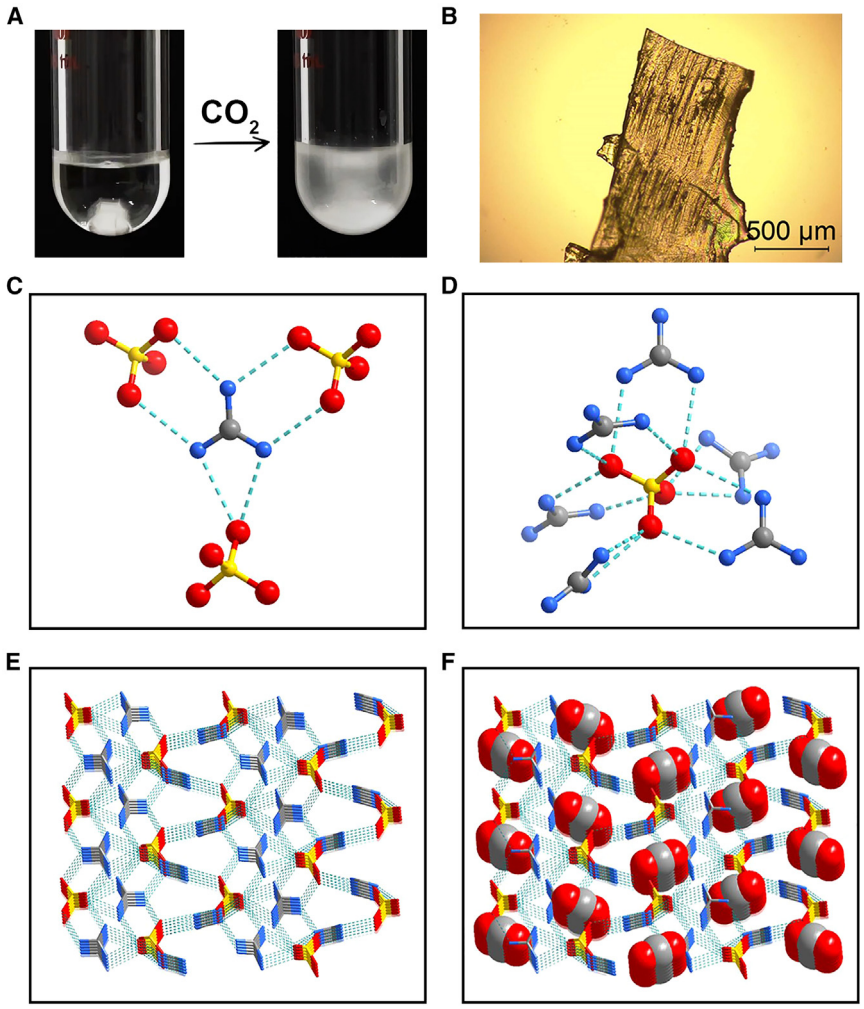

Figure 2. Formation and single-crystal structure of the clathrate, CO_2@Gua_2SO_4

(A) Photos of CO_2@Gua_2SO_4 precipitation under CO_2 atmosphere and magnetic stirring. Test tube diameter is 2.8 cm.

(B) Optical image of CO_2@Gua_2SO_4 crystal. Scale bar is 500 μm.

(C) Hydrogen-bond interactions of guanidinium cations with three SO_4^{2-} ions.

(D) Hydrogen-bond interactions of SO_4^{2-} with six guanidinium ions.

(E and F) 3D hydrogen-bonded framework of CO_2@Gua_2SO_4 omitting CO_2 (E) and (F) with captured CO_2. Dash lines represent hydrogen bonds. Hydrogen-bond interaction is deduced from single-crystal X-ray diffraction measurements. Hydrogens are omitted for clarity. Color code: gray, carbon; blue, nitrogen; red, oxygen; yellow, sulfur.

CO_2@Gua_2SO_4 are determined to be 0.252 g cm^{-3} and 17 wt %, respectively, revealing its tremendous potential for carbon capture and storage in practical conditions.

RESULTS

Synthesis and crystal structure of CO_2@Gua_2SO_4

Upon charging an aqueous Gua_2SO_4 solution with CO_2, we observe spontaneous formation of a single-crystalline CO_2@Gua_2SO_4 (see experimental procedures for details; Figure S1–S7, 2A, and 2B). The crystal structure of CO_2@Gua_2SO_4 is determined by single-crystal X-ray diffraction experiments at 100 K (Figure S2; Table S1).

In CO_2@Gua_2SO_4, each guanidinium ion adopts two sets of hydrogen bonds (H-bonds) connecting three SO_4^{2-} ions (Figure 2C), while each sulfate ion connects six guanidinium ions via multiple H-bonds (Figure 2F). The extended H-bond system (Figure S3; Table S2) in 3D results in a H-bonded framework crystallized at a tetragonal space group in which four CO_2 molecules are accommodated in each unit cell (Figures 2E, 2F, and S4). As shown in Figure S5, an irregular cage comprised of five sulfate and eight guanidinium ions can be identified, in which one CO_2 molecule is accommodated, and the cages are stacked by plane sharing. In contrast, free Gua_2SO_4 crystallizes with a cubic space group in a dense-stacking mode, in which the H-bond connection modes between Gua^+ and SO_4^{2-} ions are notably different (Figure S7).

Surprisingly enough, in CO_2@Gua_2SO_4, a H-bond interaction between CO_2 and Gua_2SO_4 is not favored because the distances and angles are out of range for a typical H-bond interaction (Figure S8), and this creates a tremendous opportunity for a reversible CO_2 capture. In a molecule of CO_2, C and O atoms bear partially positive and negative charges, respectively. The C atom exists as a carbocation and N atoms bear partial negative charge in a guanidinium cation. The distance among these oppositely charged atoms ranges from 3.4 to 3.9 Å (Figure 3A) so that the electrostatic interaction is more pronounced. One CO_2 molecule interacts with three guanidinium ions with a "triple-team structure," ensuring an effective coulombic force. The distance between positive C in CO_2 and negative O in SO_4^{2-} is determined to be 5.026 Å (Figure 3B), indicating a much weaker electrostatic interaction. We ascribe these multiple electrostatic interactions as the main driving forces for CO_2-induced crystallization of CO_2@Gua_2SO_4 from aqueous solution under CO_2 atmosphere. The solid-state magic-angle spin ^{13}C nuclear magnetic resonance (NMR) spectrum of CO_2@Gua_2SO_4 displays a sharp chemical shift at 124.9 ppm (Figure 3C), equal to the chemical shift of CO_2 in a physisorption state.[26,27] This is consistent with the result from crystal structure analysis as mentioned above. The other peak at 159.2 ppm is assigned to the carbocation in the guanidinium. A similar peak with stretching vibration of gas phase CO_2 appears in the infrared (IR) spectrum of CO_2@Gua_2SO_4 at 2,335 cm^{-1}, which also suggests the weak interaction of CO_2 with guanidinium and SO_4^{2-} ions (Figure 3D). It is worth noting that when reacting with hydroxyl and amine functional groups, CO_2 is often converted into carbonate ester or carbamate.[14–16,28] Owing to the positive charge, guanidinium cations with three amine groups interact with CO_2 via an electrostatic interaction instead of a chemical reaction. This moderate but abundant interaction is strong enough to pull guanidiniums and SO_4^{2-} together for CO_2 clathrate formation and crystallization in aqueous solution. In synthetic terms, the CO_2 inclusion mechanism unraveled by single-crystal structure analysis manifests that amino groups could interact with CO_2 via electrostatic interactions instead of a chemical reaction, owing to the delocalization of lone-pair electrons from amino functionalities to carbocations of guanidinium ions. The results point to a substantial parameter space to tune the interactions between CO_2 and sorbents for optimized carbon capture in terms of energetics and economics.

In order to screen counter anions on guanidinium, we have tested a series of guanidinium salts for CO_2 clathrate potential, including nitrate, chloride, and phosphate (see details in experimental procedures). None, however, resulted in any precipitate under the same conditions using guanidinium cations. Chloride ion is not favorable for H-bond formation,[29] while nitrate ion and guanidinium generate a plane structure, as both ions are planar,[30] and therefore not beneficial for CO_2 clathrate formation. The complicated hydrolysis process of phosphate in aqueous solution may

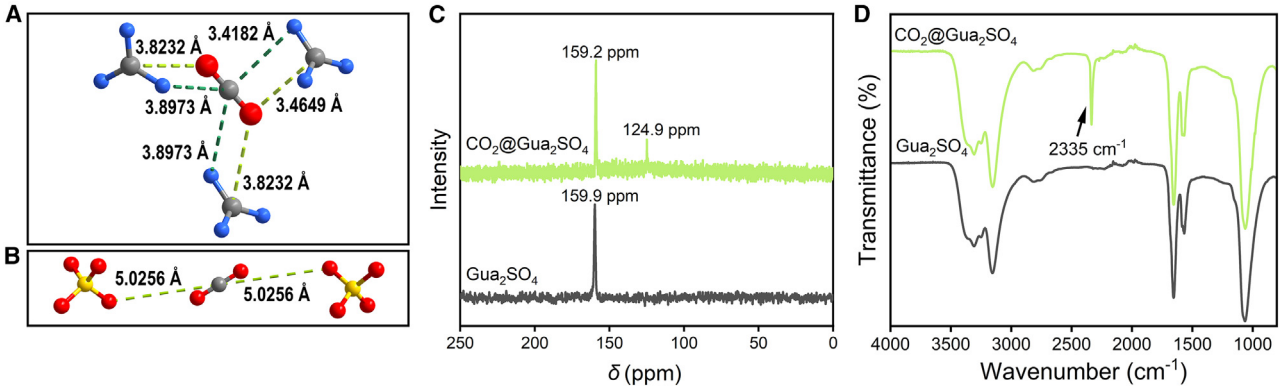

Figure 3. Interaction of CO_2 with guanidinium and sulfate ions

(A) Electrostatic interactions between CO_2 and guanidinium cations.

(B) Distance between CO_2 and sulfate ions in CO_2@Gua_2SO_4 based on single-crystal X-ray diffraction data.

(C) Solid-state magic-angle spin ^{13}C NMR spectrum of CO_2@Gua_2SO_4 and Gua_2SO_4.

(D) ATR-IR spectra of CO_2@Gua_2SO_4 and Gua_2SO_4.

account for the failure of CO_2 co-precipitation.[31] It is safe to conclude that the complex H-bond interactions between guanidinium and sulfate are crucial for crystal formation and CO_2 capture.

Optimization of CO_2 clathrate formation

In an attempt to explore the boundary conditions of CO_2@Gua_2SO_4 formation, we varied pH, Gua_2SO_4 concentration, CO_2 pressure, and temperature. Since basic aqueous solutions directly react with CO_2, we tuned the pH of Gua_2SO_4 solutions from 1 to 7 using a H_2SO_4 solution. We found that pH value has little influence over CO_2@Gua_2SO_4 formation (Figure 4A). Considering the possible influence of anion size on boundary conditions, HCl and HNO_3 were also used to adjust the pH. The results showed that the sizes of the anions exert negligible effects on the formation conditions of CO_2@Gua_2SO_4 (Figure S9). Increasing CO_2 pressure led to a higher production rate of CO_2@Gua_2SO_4 (Figure S10). The saturated Gua_2SO_4 concentration is determined to be 72 and 75.7 wt % in water at 273 and 298 K, respectively. In order to eliminate the influence of the Gua_2SO_4 concentration variation during the continuous precipitation of CO_2@Gua_2SO_4, we used a saturated solution in equilibrium with excess Gua_2SO_4 powder to investigate the temperature-pressure relationship under phase equilibrium conditions. At equilibrium, the CO_2 pressure-temperature relationship fitted well to the Clapeyron-Clausius equation (Figures 4B, S11, and S12), revealing the boundary conditions of CO_2@Gua_2SO_4 formation and indicating a wide range of conditions for capturing CO_2 using aqueous Gua_2SO_4. CO_2@Gua_2SO_4 started to crystallize at a CO_2 pressure of 32 and 52 kPa at 273 and 298 K, respectively (Figure 4B), whereas conventional CO_2 hydrates are formed under 1,500 kPa at 275 K, about 50 times higher than that of CO_2@Gua_2SO_4 formation.[32] The sorption enthalpy change for CO_2@Gua_2SO_4 is calculated to be 15.37 kJ/mol (Figure S12). This value is considerably lower than the enthalpy changes of most CO_2 absorbents as summarized in Figure S13[19,33–37] and falls into the physisorptive domain (<40 kJ/mol), suggesting minute heat requirements during CO_2 capture and release and corresponding to the ease of clathrate formation and collapse. In contrast, the enthalpy change for conventional CO_2 hydrate decomposition is 57.1 kJ/mol, owing to the necessity of breaking ample H-bonds among H_2O molecules,[32] about 3.7 times higher than that of CO_2@Gua_2SO_4.

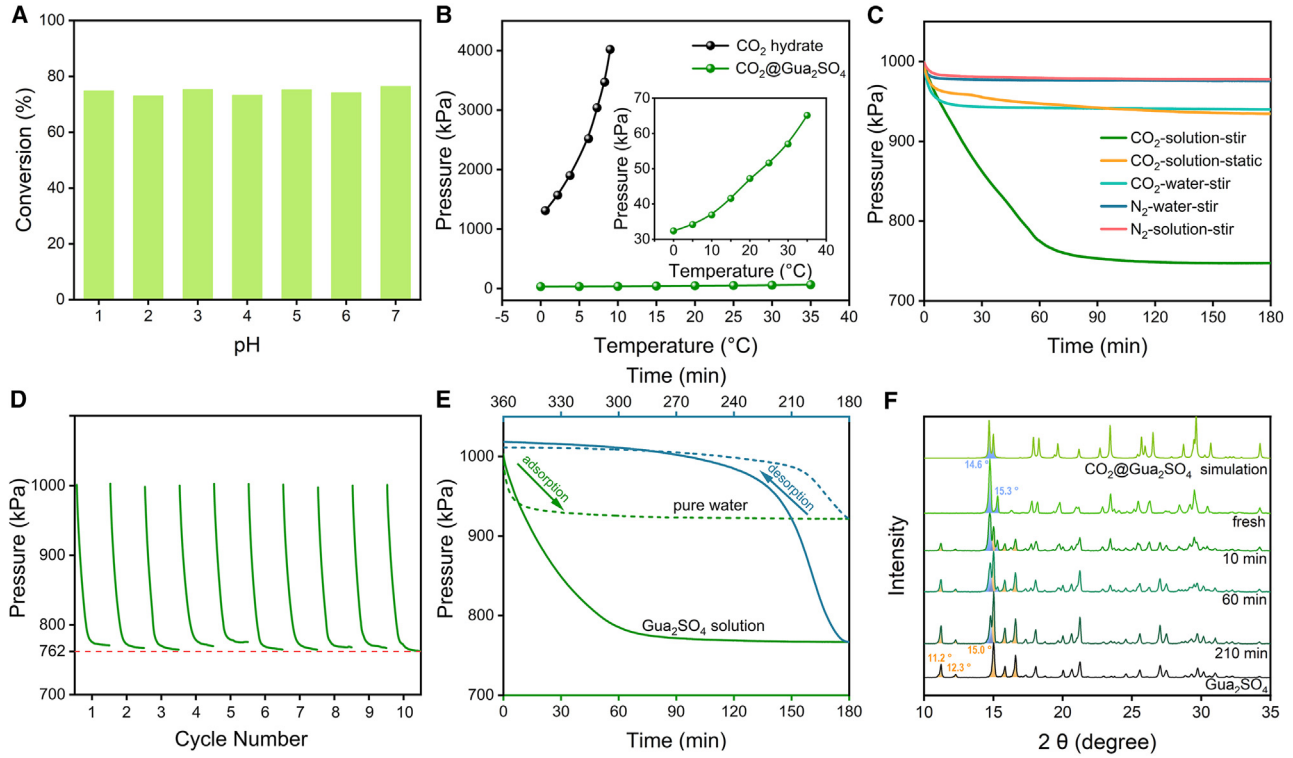

Figure 4. CO_2 sorption behavior in a Gua_2SO_4 aqueous solution

(A) pH effect on CO_2@Gua_2SO_4 formation.

(B) Pressure-temperature correlation of CO_2-Gua_2SO_4 aqueous system under equilibrium. CO_2 hydrate data is plotted as a reference.[29]

(C) CO_2 sorption profile in aqueous Gua_2SO_4 with or without stirring. CO_2 pressure changes of the control experiments, (i) CO_2 sorption in pure water with stirring, (ii) N_2 sorption in pure water, and (iii) aqueous Gua_2SO_4 with or without stirring, are given as a reference.

(D) Cyclic performance of CO_2 sorption in aqueous Gua_2SO_4. The margin of error points at a $\pm$3.5% variation.

(E) The pressure changes vs. time plot of CO_2 adsorption and desorption in water and aqueous Gua_2SO_4 with a temperature swing between 273 (adsorption) and 303 K (desorption). Dashed lines are for pure water, and solid lines represent aqueous Gua_2SO_4.

(F) PXRD data for structural evolution from CO_2@Gua_2SO_4 to Gua_2SO_4 in air. PXRD patterns of CO_2@Gua_2SO_4 simulated from crystallographic data and as-prepared Gua_2SO_4 are given for reference (peaks marked as blue and orange belong to CO_2@Gua_2SO_4 and Gua_2SO_4, respectively).

The CO_2 in CO_2@Gua_2SO_4 solidifies at near-ambient conditions with four CO_2 molecules accommodated in each unit cell with a cell volume of 1,159 Å^3, corresponding to a CO_2 volume density of 0.252 g cm^{-3}. This is equal to about 140 m^3 CO_2 in one cubic meter of CO_2@Gua_2SO_4. Gravimetrically, the CO_2 loading in CO_2@Gua_2SO_4 is calculated to be 17 wt %. As shown in Figure S14, 2.3 g CO_2 was stored in a 20 mL glass bottle, which corresponds to 1.2 L CO_2 gas at standard conditions at room temperature. In contrast, to store the same amount of CO_2 gas in a 20 mL bottle, the pressure will have to reach 6,000 kPa at 0°C. Hence, CO_2@Gua_2SO_4 is an ideal candidate for CO_2 storage and transport. Other reported CO_2 clathrates, in general, are formed under low-temperature and/or high-pressure conditions, as summarized in Table S3. The inability to operate in ambient conditions renders these clathrates not feasible for flue gas treatment, as large deviation of temperature and/or pressure from ambient conditions means substantial energy input for a practical carbon capture operation. Gua_2SO_4 is perfectly optimized for such a job, as it stores 140 m^3 CO_2 in 1 m^3 clathrate with a gravimetric capacity of 17% (uptake at 52 kPa and room temperature [RT] and release at ambient conditions), positioning it even better than most common porous materials as summarized in Table S4. And the structure does this in a simple pressure swing adsorption (PSA) cycle, eliminating energy-intensive

processes and showing quantitative capture of CO_2 in the presence of N_2 and H_2O (as discussed in the next section). It is important to note that only liquid amine solutions (industrial standard) could do such a performance with the kinetics that a process needs.

Kinetics of CO_2 clathrate formation

In an isochoric experiment, after removing air by CO_2 flushing, the stainless-steel autoclave containing Gua_2SO_4 solution (1.5 g/g, 60 wt %) was charged with CO_2 to 1,000 kPa at 273 K with constant stirring (Figure S15). The pressure drop was monitored against time, and we found that the pressure decreases in an approximatively linear fashion until 60 min and gets stable at about 100 min (Figure 4C). Replacing Gua_2SO_4 solution with pure water leads to a much smaller pressure drop. The latter is about one-fifth of the aqueous Gua_2SO_4 solution under the same conditions and results from CO_2 dissolution in water and the temperature drop from RT to 273 K. N_2, however, does not dissolve well and shows similar behavior in both pure water and Gua_2SO_4 solutions, proving that N_2 cannot form any clathrates under the same conditions. Therefore, we concluded that the structure alternate between Gua_2SO_4 and CO_2@Gua_2SO_4 exclusively for CO_2, even in the presence of N_2 and water. The final conversion yield of CO_2@Gua_2SO_4 is around 85 wt % of Gua_2SO_4 according to the weight increase of the solution.

The kinetics of CO_2@Gua_2SO_4 formation closely follows the Gua_2SO_4 concentration, CO_2 pressure, temperature, and stirring. In principle, the formation of CO_2@Gua_2SO_4 through the steps of gas dissolution, diffusion, nucleation, and growth is quite similar to a conventional CO_2 hydrate formation process.[38] In a static experiment without stirring, the CO_2 pressure drop is very low and similar to the case of gaseous CO_2 dissolution in water under the same period (Figure 4C). A crystalline layer was observed over the solution, preventing further gas diffusion. We recorded the crystallization process by sustaining a CO_2 pressure at 300 kPa while constantly stirring (Video S1). The solution is initially clear, with CO_2 dissolving and diffusing. We note that the nucleation first occurs near the vortex of stirring, which correlates to high CO_2 concentrations in the vicinity. Once the nucleation is initiated, the solution becomes turbid very quickly, owing to the rapid crystal growth. Therefore, it is safe to conclude that CO_2 dissolution and diffusion are the rate-determining steps for CO_2@Gua_2SO_4 formation.

Even though physisorptive CO_2 capture processes are well known to be durable with long cycle life, we repeated the sorption process for ten cycles, and the data exhibit excellent reproducibility, as Gua_2SO_4 is stable and nonvolatile and does not degrade or become lost during the continuous operations (Figures 4D, S16, and S17A). In a temperature swing experiment, we warmed up the autoclave to 303 K after adsorption reached equilibrium at 273 K and observed the pressure increasing (Figure 4E). This is clearly associated with CO_2@Gua_2SO_4 collapse and CO_2 release. The final pressure is slightly higher than initial value owing to the higher final temperature of the autoclave. The results reveal a reversible formation and decomposition of a salt-CO_2 clathrate accompanied by CO_2 capture and release near RT.

Cyclic CO_2 capture

The precipitates of CO_2@Gua_2SO_4 can be separated via centrifugation or a simple filtration. In open air, dry CO_2@Gua_2SO_4 decomposes with CO_2 release, as verified by powder X-ray diffraction (PXRD), but the decomposition in solid state is sluggish (Figure 4F). The PXRD of the fresh CO_2@Gua_2SO_4 sample matched well with the

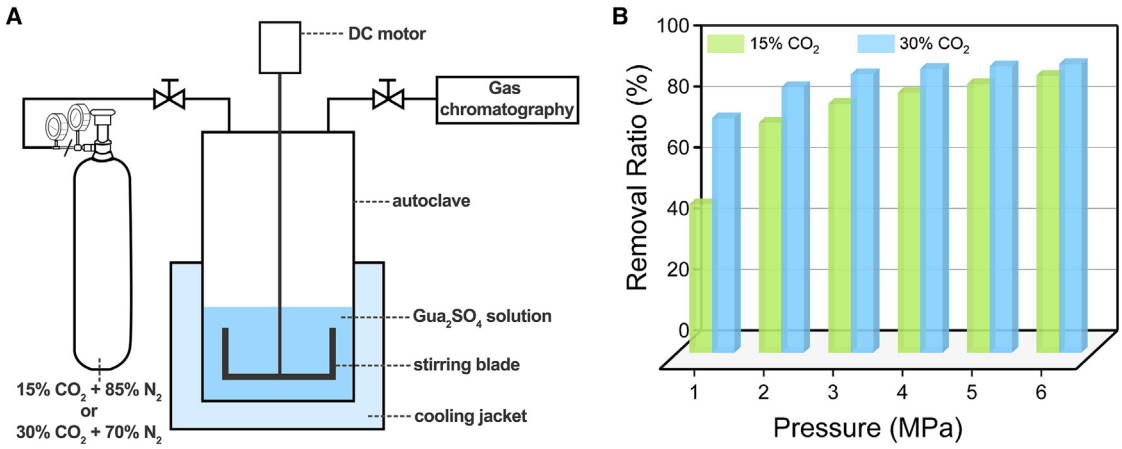

Figure 5. CO_2 removal performance of Gua_2SO_4-saturated solution with a dry simulated flue gas

(A) Schematic illustration of the setup.

(B) CO_2 removal percentages against total flue gas pressure with CO_2 mole percentages at 15 and 30 mol %.

pattern simulated from single-crystal (SC) XRD data, with some deviation at 15.0° owing to its deposition method at sample preparation and the difference of measurement temperature (Figure S6). Note that the main peaks at 14.6° and 15.3° of CO_2@Gua_2SO_4 gradually fade, while new peaks at low angles of 11.2°, 12.3°, and 15.0° belonging to the Gua_2SO_4 phase appear and grow with prolonged exposure time in air. The thermogravimetric analysis (TGA) and differential scanning calorimetry (DSC) analyses of the CO_2@Gua_2SO_4 sample in air are shown in Figure S17B. The weight loss of ca. 13.7% before 86.5°C is originated from the removal of CO_2, which is slightly less than 17% (theoretical capacity of CO_2 in CO_2@Gua_2SO_4). It can be attributed to CO_2@Gua_2SO_4 slightly decomposing with CO_2 release during sample preparation and measurements. Upon adding water to a CO_2@Gua_2SO_4 powder, we observe rapid CO_2 release with vigorous bubbling, and the solids disappear because Gua_2SO_4 salt, the only decomposition product, is highly soluble (Video S2). Judging from the shrinking solids, we project the CO_2 release proceeds from the outside in. The formed Gua_2SO_4 on the surface of CO_2@Gua_2SO_4 could block further CO_2 release and slow down the decomposition rate, but as Gua_2SO_4 is dissolved out with water, the CO_2 release remains unaltered. The decarbonized Gua_2SO_4 solid or solution is ready for reuse without requiring any further regeneration step. The released CO_2 purity from CO_2@Gua_2SO_4 is 100% except when regeneration was done by water and therefore saturated with water vapor and can be used directly in the CO_2 market including in refrigerant, beverage, pharmaceutical, and food storage sectors.

CO_2 removal from flue gas

Since CO_2 capture is conducted in an aqueous solution and moisture exerts no influence over CO_2 capture, we tested CO_2 removal performance of a Gua_2SO_4-saturated solution with a dry simulated flue gas of different molar ratios of N_2 and CO_2. The CO_2 percentage in a flue gas is typically in the range of 5%–15% depending on the industrial processes and sources.[39] With limited CO_2 partial pressure, we pressurized flue gas in order to reach a high CO_2 presence. A schematic illustration of setup is shown in Figure 5A. Figure 5B and Table S5 summarize CO_2 capture performances at varying total flue gas pressures. Obviously, the higher pressure leads to higher CO_2 removal. In the case of a CO_2 percentage at 15%, total flue gas needs to be pressurized to 5,000–6,000 kPa to meet DOE targets in terms of a 90% CO_2

capture. When the CO_2 percentage is increased to 30% (i.e., from the cement industry), the flue gas pressure can be as low as 2,000–3,000 kPa for a 90% CO_2 removal. We also note that the CO_2 content in natural gas streams can reach over 40% in some cases.[40] The high CO_2 content will lower the total pressure of mixtures and therefore reduce the CO_2 removal cost based on the physisorptive clathrate mechanism of the CO_2@Gua_2SO_4.

DISCUSSION

In this work, we reported the first ambient example of mimicking CO_2 hydrate structure with CO_2 as guest molecules. A simple Gua_2SO_4 co-crystallizes with CO_2 into a stable clathrate (CO_2@Gua_2SO_4). The clathrate releases CO_2 on demand, and both adsorption and desorption can occur at mild conditions. The H-bonded framework assembled from guanidinium and sulfate mimics the water cage in a CO_2 hydrate, effectively trapping four CO_2 molecules per unit cell of the clathrate. Electrostatic interactions between guanidinium ion and CO_2 are revealed through a single crystal (SC) study instead of the van der Waals interactions commonly observed for CO_2 and water cages of CO_2 hydrates.

The *in situ* process of co-crystallization introduced here is fundamentally different from CO_2 adsorption in a preformed H-bonded organic framework and is quite unlike CO_2 physisorption in other porous materials. A CO_2 clathrate imitating the CO_2 hydrate, therefore, exhibits unique advantages toward carbon capture. First, Gua_2SO_4 exclusively captures CO_2 without water or moisture interference, swiftly overcoming the fatal weakness of any physisorption processes. Second, CO_2 release through structure collapsing could be triggered at ambient conditions, requiring little energy input for absorbent regeneration while defeating the parasitic energy dilemma of chemisorption. Third, Gua_2SO_4 is stable and noncorrosive, a highly desirable feature when compared with ethanol amine, ammonia, and other basic solutions that are commonly used in carbon capture. Fourth, a stable CO_2@Gua_2SO_4 in powder form is also beneficial for storage and transportation of CO_2, benefiting from its remarkably high volume per weight capacity. In addition, by the lessons learned in this study, we can tune dynamic H-bonded frameworks with enriched structural variation, enabling us further to regulate and control the properties for further improving CO_2 capture in terms of stability, recyclability, sorption capacity, and selectivity, while lowering regeneration energy penalty and cost.

EXPERIMENTAL PROCEDURES

Resource availability

Lead contact

Further information and request for the resources are available from the lead contact, Bo Liu (liuchem@ustc.edu.cn).

Materials availability

No unique materials were generated by this study.

Data and code availability

Crystallographic data for the key structure, CO_2@Gua_2SO_4, reported in this article is available from the Cambridge Crystallographic Data Centre with CCDC: 2092196. Copies of the data can be obtained free of charge via https://www.ccdc.cam.ac.uk/structures/ or from a direct link. All other data that support the findings of this study are available in the article and supplemental information.

Materials

All chemicals and reagents were purchased from commercial suppliers and used without further purification. Deionized water was used as solvent. Ethanol and sulfuric acid were purchased from Sinopharm Chemical Reagent. Guanidinium carbonate (Gua_2CO_3) was purchased from Shanghai Adamas Reagent. Nitrogen gas (99.999%), carbon dioxide (99.9%), and carbon dioxide-nitrogen mixture gas (15 mol % CO_2+85 mol % N_2 and 30 mol % CO_2+70 mol % N_2) were purchased from Nanjing Special Gas Plant.

Characterization

PXRD measurements were conducted on a Rigaku MiniFlex 600 diffractometer using Cu Kα radiation (λ = 1.5418 Å). The FTIR spectrum was measured by a Nicolet iS5 spectrophotometer with an attenuated total reflectance (ATR) module (Thermo Fisher Scientific, Waltham, MA, USA). Solid-state NMR spectra were recorded by a Bruker AVANCE *NEO* 600WB spectrometer with a magic-angle spin (MAS) rate of 15 kHz. The ^{13}C resonance frequency was 150.93 MHz at the experiment. ^{13}C single-pulse spectrum was recorded with 16 s pulse delay. TGAs were performed from 25°C to 800°C at a heating rate of 10°C/min in air on a TGA Q500 integration thermal analyzer (For CO_2@Gua_2SO_4, the heating rate from 20°C to 300°C was 5°C/min and from 300°C to 700°C, 10°C/min). Gas chromatography (GC) was performed on a Shimadzu GC 2014 gas chromatograph fitted with a Porapak Q column and TCD detector. Ar gas (99.999%) was used as the carrier gas.

Synthesis of Gua_2SO_4

Gua_2SO_4 was synthesized simply by neutralizing guanidinium carbonate with H_2SO_4. Gua_2CO_3 (180 g, 1 mol) and deionized water (250 mL) were first mixed in a 1,000 mL beaker. Concentrated H_2SO_4 (98%, 54 mL, 1 mol) was then added dropwise into the beaker at a rate of one drop per second. The final pH was adjusted to 7 using only H_2SO_4. Absolute ethanol was added as nonsolvent under constant stirring to precipitate the product. The colorless powder was collected by vacuum filtration, followed by washing with absolute ethanol and drying in an oven at 100°C before use. Yield was calculated to be 99% based on guanidinium. The production of Gua_2SO_4 was verified by common characterization tools, particularly PXRD (Figure S1).

Synthesis of CO_2@Gua_2SO_4 SC

A CO_2@Gua_2SO_4 SC was grown by treating an aqueous Gua_2SO_4 solution with CO_2 at low temperature. Gua_2SO_4 (3 g) was dissolved in water (5 mL). After complete dissolution, the solution was added in a glass vial, which was placed in an autoclave. The autoclave was rinsed using CO_2 to completely replace the air, and the final CO_2 pressure in the autoclave was fixed at 700 kPa. The autoclave was kept at 2°C by a cooling jacket. Colorless plate-like SCs at centimeter sizes were obtained after 12 h.

SC XRD measurements

Since the crystals of CO_2@Gua_2SO_4 readily decompose at atmospheric conditions, a fresh crystal from the reactor was placed on top of a glass fiber under a stream of liquid nitrogen and rapidly mounted onto a sample goniometer for centering. SC XRD data were collected by a Rigaku Oxford Diffraction Super-Nova diffractometer using Mo-Kα radiation (λ = 0.71073 Å) at 100 K. The data collection and processing were carried out with CrysAlisPro software. The crystal structure was solved by direct method and refined by full-matrix least squares based on F^2 using an SHELXTL 14XL program package. Hydrogen atoms were fixed geometrically at their positions and allowed to ride on parent atoms. Crystallographic and structure refinements data for CO_2@Gua_2SO_4 are summarized in Table S1.

PXRD of CO_2@Gua_2SO_4

RT PXRD spectra of CO_2@Gua_2SO_4 slightly deviated from the simulated one especially at (004) plane (Figures S5 and S6) because the measurements were conducted at different temperatures. At 100 K, the guest CO_2 molecules stopped moving and therefore were forced to align with guanidinium to maximize the H-bonding interactions. At RT, however, the CO_2 molecules were in free motion, leading to an expected disorder. Detailed analysis from the crystal structure indicates that CO_2 molecules are predominantly located in the (004) plane. Therefore, the peak position of the (004) plane in PXRD at RT shifts to a higher 2θ when CO_2 is released (Figure S5).

The effect of counter ions on formation of CO_2 clathrate

A series of guanidinium salts were selected to be tested, including guanidine hydrochloride, guanidine nitrate, and guanidine dihydrogen phosphate. Saturated solutions of guanidinium salts were added into glass vials, which were separately placed in an autoclave. The air in the autoclave was exchanged with CO_2 at least three times before the CO_2 pressure inside was fixed at 1,000 kPa (10 bar). The autoclave was kept at 0°C, controlled by a cooling jacket. After 24 h with continuous stirring, glass vials were checked for any precipitation.

The pH influence on CO_2 adsorption

The pH value of Gua_2SO_4 aqueous solution is determined to be 7. The pH values of a series of Gua_2SO_4 solutions (73.7 wt %) were set at 1, 2, 3, 4, 5, and 6 using H_2SO_4, HCl, and HNO_3 solutions. Solutions were then charged into separate glass vials and weighed. The vials were put in an autoclave that was already connected to a CO_2 cylinder. The air in the autoclave was exchanged with CO_2 at least three times before the CO_2 pressure inside was fixed at 1,000 kPa (10 bar). The temperature of the autoclave was kept at 0°C using a cooling jacket. After 12 h of constant stirring, the pressure was recorded, and the vial containing Gua_2SO_4 aqueous solution was weighed again to calculate the adsorbed amount of CO_2. Note that the dissolved CO_2 was ignored in calculations, as the CO_2 dissolved in solution is negligible (1.44 mg/g at 25°C) compared with that of the amount adsorbed by Gua_2SO_4.

The effect of pressure on the CO_2 uptake of Gua_2SO_4

A Gua_2SO_4 aqueous solution (60 wt %, 1.5 g/g) was charged into a glass vial and weighed. The vial was put into autoclave that was connected to a CO_2 cylinder. The air in the autoclave was exchanged with CO_2 at least three times before the CO_2 pressure inside was set to the desired values. The temperature of the autoclave was kept at 0°C using a cooling jacket. After 12 h of continuous stirring, the pressure was recorded, and the vial containing Gua_2SO_4 aqueous solution was weighed again to calculate the conversion rate. Note that the dissolved CO_2 was ignored in the conversion calculations, as the CO_2 dissolved in solution is negligible compared with that of the amount adsorbed by Gua_2SO_4.

CO_2 equilibrium pressures of CO_2-Gua_2SO_4 aqueous solutions at various temperatures

A saturated Gua_2SO_4 solution at 40°C (10 mL) and 2 g Gua_2SO_4 powder was mixed in a 100 mL autoclave under constant stirring. The temperature of the autoclave was kept at 0°C using a cooling jacket. The autoclave was evacuated under vacuum and filled with CO_2. The flushing was repeated three times to completely remove air from the autoclave. Then, the autoclave was charged with CO_2 to 100 kPa (1 bar). The pressure drop was monitored until readings were steady. The final pressure value was taken as the equilibrium pressure at the set temperature (0°C, 5°C, 10°C, 15°C, 20°C, 25°C, and 30°C). The water vapor pressure of a saturated

Gua_2SO_4 solution was also measured under the same conditions. CO_2 equilibrium pressure was obtained by subtracting the water vapor pressure at the same temperature from the recorded total pressure and plotted against temperature (Figure S11).

Cycling sorption experiments

2.5 g Gua_2SO_4 was dissolved in a glass vial with 2 mL water. The vial was put in a 100 mL autoclave, and the temperature was kept at 0°C using a jacket-cooling system. The air in the autoclave was exchanged with CO_2 at least three times before the CO_2 pressure inside was set to 1,000 kPa (10 bar). The pressure was monitored using a digital pressure meter (5 s per point) with constant stirring. After the pressure stabilized, the chamber was vented, and white slurry was observed in the vial. Ultrasound was then applied to decompose the product and release CO_2, with a rush of bubbles indicating the decomposition process. The procedure was repeated to test the cyclic performance of CO_2 adsorption for at least ten runs. After the final cycle, absolute ethanol was added to the solution, and a precipitate was obtained, which was subsequently dried at 100°C. The PXRD of the precipitate is consistent with that of the pristine Gua_2SO_4 (Figure S14). The conversion rate was determined gravimetrically by weighing the Gua_2SO_4 aqueous solution before and after CO_2 adsorptions. The conversion rate can also be calculated according to the CO_2 pressure drop during the sorption process. Control experiments were conducted following the same procedure but using pure water instead of Gua_2SO_4 aqueous solution, and N_2 gas instead of CO_2, and with or without stirring.

Isochoric adsorption-desorption experiments

2.5 g Gua_2SO_4 was dissolved in a glass vial with 2 mL water. The vial was put in a 100 mL autoclave, and the temperature was kept at 0°C using a jacket-cooling system. The air in the autoclave was exchanged with CO_2 at least three times before the CO_2 pressure inside was set to 1,000 kPa (10 bar). The pressure was monitored using a digital pressure meter (5 s per point) with constant stirring. After 3 h, the pressure became stable. Then, the temperature of the autoclave was increased to 30°C using a water bath, and the pressure inside the autoclave was recorded.

CO_2 removal from flue gas

Owing to the relatively high viscousity of concentrated Gua_2SO_4 solutions, an autoclave equipped with mechanical stirring was used in this experiment to speed up CO_2 dissolution and diffusion. Gua_2SO_4 (27 g) and water (7 mL) were charged into the autoclave. The air in the autoclave was first exchanged with flue gas three times before setting the gas pressure inside to a specific value. The temperature of the autoclave was kept at 0°C using a cooling jacket. CO_2 content after the sorption for 24 h was analyzed by a GC. The removal percentage of flue gas under different pressure is shown in Table S5.

SUPPLEMENTAL INFORMATION

Supplemental information can be found online at https://doi.org/10.1016/j.xcrp.2023.101383.

ACKNOWLEDGMENTS

We acknowledge support from the Chinese Academy of Sciences, the National Key Research and Development Program of China (2021YFA1500402), the National Natural Science Foundation of China (NSFC; 21571167, 51502282, and 22075266), and

the Fundamental Research Funds for the Central Universities (WK2060190053 and WK2060190100).

AUTHOR CONTRIBUTIONS

B.L. conceived of the idea, and B.L., Q.X., and C.T.Y. supervised the project together. Z.X. designed and carried out the experiments. C.L., X.X., and T.S.N. contributed to data analysis and manuscript preparation. C.C. collected SC XRD data and solved the structure. B.L., Q.X., and C.T.Y. wrote the manuscript together. All authors discussed the results and assisted with manuscript preparation.

DECLARATION OF INTERESTS

C.T.Y. is an advisory board member at *Cell Reports Physical Science*. USTC filed one Chinese patent (application #202210271224.0) from the data reported in this study.

Received: January 8, 2023
Revised: March 6, 2023
Accepted: March 29, 2023
Published: April 21, 2023

REFERENCES

1. Singh, G., Lakhi, K.S., Sil, S., Bhosale, S.V., Kim, I., Albahily, K., and Vinu, A. (2019). Biomass derived porous carbon for CO_2 capture. Carbon *148*, 164–186. https://doi.org/10.1016/j.carbon.2019.03.050.

2. Qi, S.-C., Liu, Y., Peng, A.-Z., Xue, D.-M., Liu, X., Liu, X.-Q., and Sun, L.-B. (2019). Fabrication of porous carbons from mesitylene for highly efficient CO_2 capture: a rational choice improving the carbon loop. Chem. Eng. J. *361*, 945–952. https://doi.org/10.1016/j.cej.2018.12.167.

3. Kumar, S., Srivastava, R., and Koh, J. (2020). Utilization of zeolites as CO_2 capturing agents: advances and future perspectives. J. CO_2 Util. *41*, 101251. https://doi.org/10.1016/j.jcou.2020.101251.

4. Panda, D., Kumar, E.A., and Singh, S.K. (2020). Introducing mesoporosity in zeolite 4A bodies for rapid CO_2 capture. J. CO2 Util. *40*, 101223. https://doi.org/10.1016/j.jcou.2020.101223.

5. Banerjee, R., Phan, A., Wang, B., Knobler, C., Furukawa, H., O'Keeffe, M., and Yaghi, O.M. (2008). High-throughput synthesis of zeolitic imidazolate frameworks and application to CO_2 capture. Science *319*, 939–943. https://doi.org/10.1126/science.1152516.

6. Sumida, K., Rogow, D.L., Mason, J.A., McDonald, T.M., Bloch, E.D., Herm, Z.R., Bae, T.-H., and Long, J.R. (2012). Carbon dioxide capture in metal–organic frameworks. Chem. Rev. *112*, 724–781. https://doi.org/10.1021/cr2003272.

7. Boyd, P.G., Chidambaram, A., García-Díez, E., Ireland, C.P., Daff, T.D., Bounds, R., Gładysiak, A., Schouwink, P., Moosavi, S.M., Maroto-Valer, M.M., et al. (2019). Data-driven design of metal–organic frameworks for wet flue gas CO_2 capture. Nature *576*, 253–256. https://doi.org/10.1038/s41586-019-1798-7.

8. Zeng, Y., Zou, R., and Zhao, Y. (2016). Covalent organic frameworks for CO_2 capture. Adv. Mater. *28*, 2855–2873. https://doi.org/10.1002/adma.201505004.

9. Wang, H., Li, B., Wu, H., Hu, T.-L., Yao, Z., Zhou, W., Xiang, S., and Chen, B. (2015). A flexible microporous hydrogen-bonded organic framework for gas sorption and separation. J. Am. Chem. Soc. *137*, 9963–9970. https://doi.org/10.1021/jacs.5b05644.

10. Shi, Z., Tao, Y., Wu, J., Zhang, C., He, H., Long, L., Lee, Y., Li, T., and Zhang, Y.-B. (2020). Robust metal–triazolate frameworks for CO_2 capture from flue gas. J. Am. Chem. Soc. *142*, 2750–2754. https://doi.org/10.1021/jacs.9b12879.

11. Cadiau, A., Belmabkhout, Y., Adil, K., Bhatt, P.M., Pillai, R.S., Shkurenko, A., Martineau-Corcos, C., Maurin, G., and Eddaoudi, M. (2017). Hydrolytically stable fluorinated metal-organic frameworks for energy-efficient dehydration. Science *356*, 731–735. https://doi.org/10.1126/science.aam8310.

12. McDonald, T.M., Mason, J.A., Kong, X., Bloch, E.D., Gygi, D., Dani, A., Crocellà, V., Giordanino, F., Odoh, S.O., Drisdell, W.S., et al. (2015). Cooperative insertion of CO_2 in diamine-appended metal-organic frameworks. Nature *519*, 303–308. https://doi.org/10.1038/nature14327.

13. Lin, J.-B., Nguyen, T.T.T., Vaidhyanathan, R., Burner, J., Taylor, J.M., Durekova, H., Akhtar, F., Mah, R.K., Ghaffari-Nik, O., Marx, S., et al. (2021). A scalable metal-organic framework as a durable physisorbent for carbon dioxide capture. Science *374*, 1464–1469. https://doi.org/10.1126/science.abi7281.

14. Laddha, S.S., and Danckwerts, P.V. (1981). Reaction of CO_2 with ethanolamines: kinetics from gas-absorption. Chem. Eng. Sci. *36*, 479–482. https://doi.org/10.1016/0009-2509(81)80135-2.

15. Yu, J., and Chuang, S.S.C. (2017). The role of water in CO_2 capture by amine. Ind. Eng. Chem. Res. *56*, 6337–6347. https://doi.org/10.1021/acs.iecr.7b00715.

16. Yang, X., Rees, R.J., Conway, W., Puxty, G., Yang, Q., and Winkler, D.A. (2017). Computational modeling and simulation of CO_2 capture by aqueous amines. Chem. Rev. *117*, 9524–9593. https://doi.org/10.1021/acs.chemrev.6b00662.

17. Seipp, C.A., Williams, N.J., Kidder, M.K., and Custelcean, R. (2017). CO_2 capture from ambient air by crystallization with a guanidine sorbent. Angew Chem. Int. Ed. Engl. *129*, 1062–1065. https://doi.org/10.1002/ange.201610916.

18. Brethomé, F.M., Williams, N.J., Seipp, C.A., Kidder, M.K., and Custelcean, R. (2018). Direct air capture of CO_2 via aqueous-phase absorption and crystalline-phase release using concentrated solar power. Nat. Energy *3*, 553–559. https://doi.org/10.1038/s41560-018-0150-z.

19. Williams, N.J., Seipp, C.A., Brethomé, F.M., Ma, Y.-Z., Ivanov, A.S., Bryantsev, V.S., Kidder, M.K., Martin, H.J., Holguin, E., Garrabrant, K.A., and Custelcean, R. (2019). CO_2 capture via crystalline hydrogen-bonded bicarbonate dimers. Chem *5*, 719–730. https://doi.org/10.1016/j.chempr.2018.12.

20. Custelcean, R., Williams, N.J., Wang, X., Garrabrant, K.A., Martin, H.J., Kidder, M.K., Ivanov, A.S., and Bryantsev, V.S. (2020). Dialing in direct air capture of CO_2 by crystal engineering of bisiminoguanidines. ChemSusChem *13*, 6381–6390. https://doi.org/10.1016/j.chempr.2018.12.025.

21. Cullen, D.A., Gardiner, M.G., and White, N.G. (2019). A three dimensional hydrogen bonded organic framework assembled through antielectrostatic hydrogen bonds. Chem. Commun. *55*, 12020–12023. https://doi.org/10.1039/C9CC06707H.

22. Sloan, E.D., and Koh, C.A. (2007). Clathrate Hydrates of Natural Gases (CRC press). https://doi.org/10.1201/9781420008494.

23. Sum, A.K., Koh, C.A., and Sloan, E.D. (2009). Clathrate hydrates: from laboratory science to engineering practice. Ind. Eng. Chem. Res. *48*, 7457–7465. https://doi.org/10.1021/ie900679m.

24. Hassanpouryouzband, A., Joonaki, E., Vasheghani Farahani, M., Takeya, S., Ruppel, C., Yang, J., English, N.J., Schicks, J.M., Edlmann, K., Mehrabian, H., et al. (2020). Gas hydrates in sustainable chemistry. Chem. Soc. Rev. *49*, 5225–5309. https://doi.org/10.1039/C8CS00989A.

25. Wang, Y., Hou, X., Liu, C., Albolkany, M.K., Wang, Y., Wu, N., Chen, C., and Liu, B. (2020). Combustible ice mimicking behavior of hydrogen-bonded organic framework at ambient condition. Nat. Commun. *11*, 3124. https://doi.org/10.1038/s41467-020-16976-1.

26. Kong, X., Scott, E., Ding, W., Mason, J.A., Long, J.R., and Reimer, J.A. (2012). CO_2 dynamics in a metal–organic framework with open metal sites. J. Am. Chem. Soc. *134*, 14341–14344. https://doi.org/10.1021/ja306822p.

27. Lin, L.-C., Kim, J., Kong, X., Scott, E., McDonald, T.M., Long, J.R., Reimer, J.A., and Smit, B. (2013). Understanding CO_2 dynamics in metal–organic frameworks with open metal sites. Angew. Chem. *125*, 4506–4509. https://doi.org/10.1002/ange.201300446.

28. Sampaio, R.N., Grills, D.C., Polyansky, D.E., Szalda, D.J., and Fujita, E. (2019). Unexpected roles of triethanolamine in the photochemical reduction of CO_2 to formate by ruthenium complexes. J. Am. Chem. Soc. *142*, 2413–2428. https://doi.org/10.1002/anie.201300446.

29. Haas, D.J., Harris, D.R., and Mills, H.H. (1965). The crystal structure of guanidinium chloride. Acta Crystallogr. *19*, 676–679. https://doi.org/10.1107/S0365110X65004085.

30. Katrusiak, A., and Szafrański, M. (1994). Guanidinium nitrate. Acta Crystallogr. C *50*, 1161–1163. https://doi.org/10.1107/S0108270193012272.

31. Li, C., Ma, J., Shen, J., and Wang, P. (2009). Removal of phosphate from secondary effluent with Fe^{2+} enhanced by H_2O_2 at nature pH/neutral pH. J. Hazard Mater. *166*, 891–896. https://doi.org/10.1016/j.jhazmat.2008.11.111.

32. Fan, S.-S., and Guo, T.-M. (1999). Hydrate formation of CO_2-rich binary and quaternary gas mixtures in aqueous sodium chloride solutions. J. Chem. Eng. Data *44*, 829–832. https://doi.org/10.1021/je990011b.

33. Galindo, P., Schäffer, A., Brechtel, K., Unterberger, S., and Scheffknecht, G. (2012). Experimental research on the performance of CO_2-loaded solutions of MEA and DEA at regeneration conditions. Fuel *101*, 2–8. https://doi.org/10.1016/j.fuel.2011.02.005.

34. Gurkan, B.E., de la Fuente, J.C., Mindrup, E.M., Ficke, L.E., Goodrich, B.F., Price, E.A., Schneider, W.F., and Brennecke, J.F. (2010). Equimolar CO_2 absorption by anion-functionalized ionic liquids. J. Am. Chem. Soc. *132*, 2116–2117. https://doi.org/10.1021/ja909305t.

35. Lee, Y., Lee, S., Lee, J., and Seo, Y. (2014). Structure identification and dissociation enthalpy measurements of the CO_2+ N_2 hydrates for their application to CO_2 capture and storage. Chem. Eng. J. *246*, 20–26. https://doi.org/10.1016/j.cej.2014.02.045.

36. Caskey, S.R., Wong-Foy, A.G., and Matzger, A.J. (2008). Dramatic tuning of carbon dioxide uptake via metal substitution in a coordination polymer with cylindrical pores. J. Am. Chem. Soc. *130*, 10870–10871. https://doi.org/10.1021/ja8036096.

37. Cavenati, S., Grande, C.A., and Rodrigues, A.E. (2004). Adsorption equilibrium of methane, carbon dioxide, and nitrogen on zeolite 13X at high pressures. J. Chem. Eng. Data *49*, 1095–1101. https://doi.org/10.1021/je0498917.

38. Bishnoi, P., and Natarajan, V. (1996). Formation and decomposition of gas hydrates. Fluid Phase Equil. *117*, 168–177. https://doi.org/10.1016/0378-3812(95)02950-8.

39. Khalilpour, R., Mumford, K., Zhai, H., Abbas, A., Stevens, G., and Rubin, E.S. (2015). Membrane-based carbon capture from flue gas: a review. J. Clean. Prod. *103*, 286–300. https://doi.org/10.1016/j.jclepro.2014.10.050.

40. Kidnay, A.J., and Parrish, W.R. (2006). Fundamentals of Natural Gas Processing (CRC press). https://doi.org/10.1201/9781420014044.